vibration

MDPI

Article

Finite Element Analysis versus Empirical Modal Analysis of a Basketball Rim and Backboard

Daniel Winarski [1,*], Kip P. Nygren [2] and Tyson Winarski [3]

[1] Independent Researcher, Tucson, AZ 85710, USA
[2] Independent Researcher, Wilmington, NC 28405, USA; kip.nygren@gmail.com
[3] Sandra Day O'Conner College of Law, Phoenix Campus, Arizona State University, Phoenix, AZ 85004, USA; tyson.winarski@asu.edu
* Correspondence: winarskifirm@gmail.com

Abstract: The first goal of this research was to document the process of using the MODAL analysis system of the ANSYS 2024R1 student edition to create a finite element model of the modes and frequencies of vibration of one basketball rim and backboard design. This finite element model included the use of steel for the rim and its mount, a tempered glass backboard, and an aluminum frame behind the backboard. After a mesh was created, fixed support boundary conditions were applied to the four corners of the aluminum frame, followed by the theoretical modal analysis. The second goal was to validate this model by comparing the finite element calculated mode shapes and frequencies to the empirical modal analysis previously measured at the United States Military Academy at West Point, New York. Five mode shapes and frequencies agreed rather well between the theoretical finite element analysis and previously published empirical modal analysis, specifically where the rim was vibrating in the vertical direction, which was the direction that the accelerometer was aligned for the empirical modal analysis. These five modes were addressed from a finite element model validation standpoint by a 99.5% confidence in a 98.09% cross-correlation with empirical modal analysis data, and from a verification standpoint by employing a refined-mesh. However, three theoretical mode shapes missed by the empirical modal analysis were found where the vibration of the rim was confined to the horizontal plane, which was orthogonal to the orientation of our accelerometer.

Keywords: mode shape; frequency; finite element analysis; modal analysis; basketball

check for updates

Citation: Winarski, D.; Nygren, K.P.; Winarski, T. Finite Element Analysis versus Empirical Modal Analysis of a Basketball Rim and Backboard. *Vibration* **2024**, *7*, 582–594. https://doi.org/10.3390/vibration7020030

Academic Editors: Delphine Chadefaux and Aleksandar Pavic

Received: 22 April 2024
Revised: 18 May 2024
Accepted: 5 June 2024
Published: 7 June 2024

Copyright: © 2024 by the authors. Licensee MDPI, Basel, Switzerland. This article is an open access article distributed under the terms and conditions of the Creative Commons Attribution (CC BY) license (https://creativecommons.org/licenses/by/4.0/).

1. Introduction

This study was inspired by the work of Javorski [1], who first characterized the dynamic behavior of a ceiling-mounted basketball goal using an impact hammer and a fixed-location accelerometer, and then compared that empirical analysis to a theoretical finite element analysis. Empirical vibration measurements were taken at fourteen nodes, ten of which were on the frame supporting the basketball rim and backboard. Only four nodes were measured on the backboard, at the corners of the backboard, and none on the rim itself. Overall, 36 frequency response functions were measured, and this study concentrated mostly on structural vibrations between 2 and 10 Hz. Thus, this important study was focused more on the structural support of the backboard and rim rather than the elastic vibrations of the backboard and rim themselves. Our goal was to follow Javorski's lead and see how many empirical modal frequency and mode shapes of the basketball rim and backboard which we could match with our theoretical finite element analysis.

ANSYS was chosen as our finite element package of choice for two major reasons. The first reason was that bundled education on this package was available online through Cornell University [2]. MAE-141 taught the conceptual foundations of finite element analysis, MAE-142 taught ANSYS mechanical concepts and implementation, MAE 143 taught elasticity applications, and MAE-144 taught beam and shell applications. Most

importantly, the final module in this bundle, MAE-145, taught vibration applications, which was very helpful. Each of these five modules contained lecture materials, quizzes, and a comprehensive hands-on student project. In this course, emphasis was placed on using the ANSYS Tree Outline to organize one's efforts, which we fully adopted along with all methodology taught. The second reason was the free ANSYS 2024R1 student edition [3].

Another important source to get us pointed in the right direction was the basketball rim and backboard modeled in ANSYS by Tickoo [4]. Tickoo's modeling did not use the precise dimensions as specified by the NCAA [5] or Gared [6]. However, he did get us started using DesignModeler within ANSYS for creating our geometry. We followed his lead of first creating the toroidal rim. Secondly, we followed his process of creating a new offset plane, followed by sketching a rectangle (saw icon), then extruding that rectangle from the offset plane to the toroidal rim to create the top of the mount. Finally, we followed his process of creating yet another new offset plane, followed by sketching yet another rectangle (saw icon), then extruding that rectangle from that second new plane to create the back of the mount. The use of ANSYS to study plate vibrations by Nkounhawa et al. [7] and Guguloth et al. [8] were also very helpful.

2. Materials and Methods

We first launched ANSYS Workbench 2024R1, then double clicked on MODAL under Analysis Systems in Workbench. This caused the MODAL cell to be displayed in the project schematic window. We then right clicked on Geometry within MODAL and selected DesignModeler Geometry from the menu. We used English units because all of the dimensions of the basketball rim, mount, and backboard are specified in inches in the United States. Figures 1–3 define how we established the geometry for the rim, its mount, the backboard, and the aluminum frame.

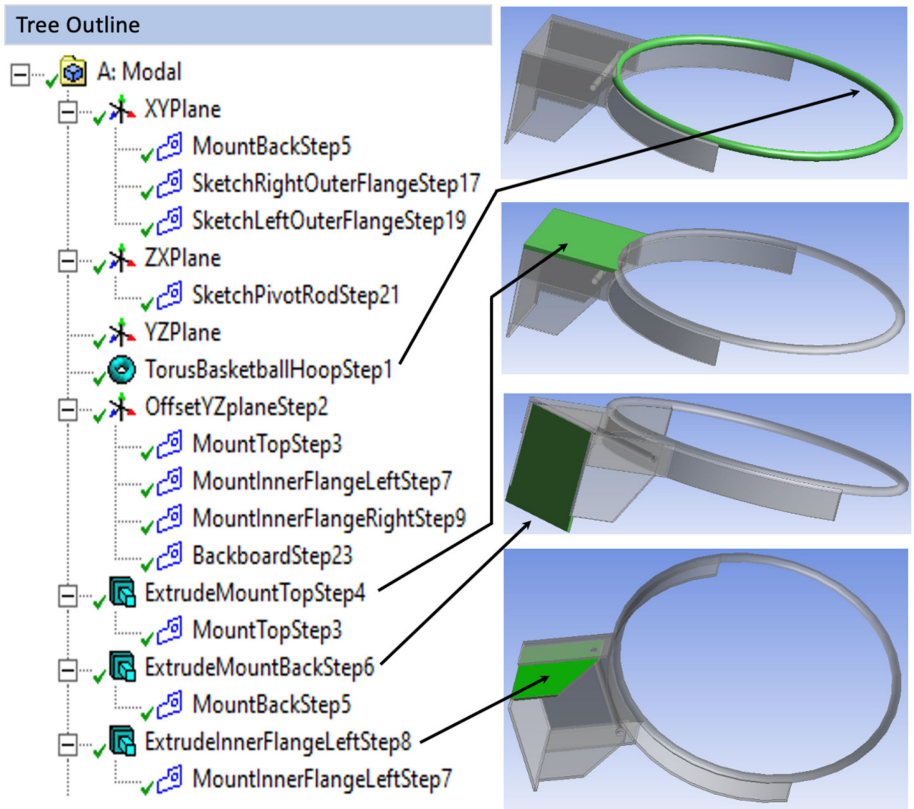


Figure 1. DesignModeler Geometry—Tree Outline 1-of-3.

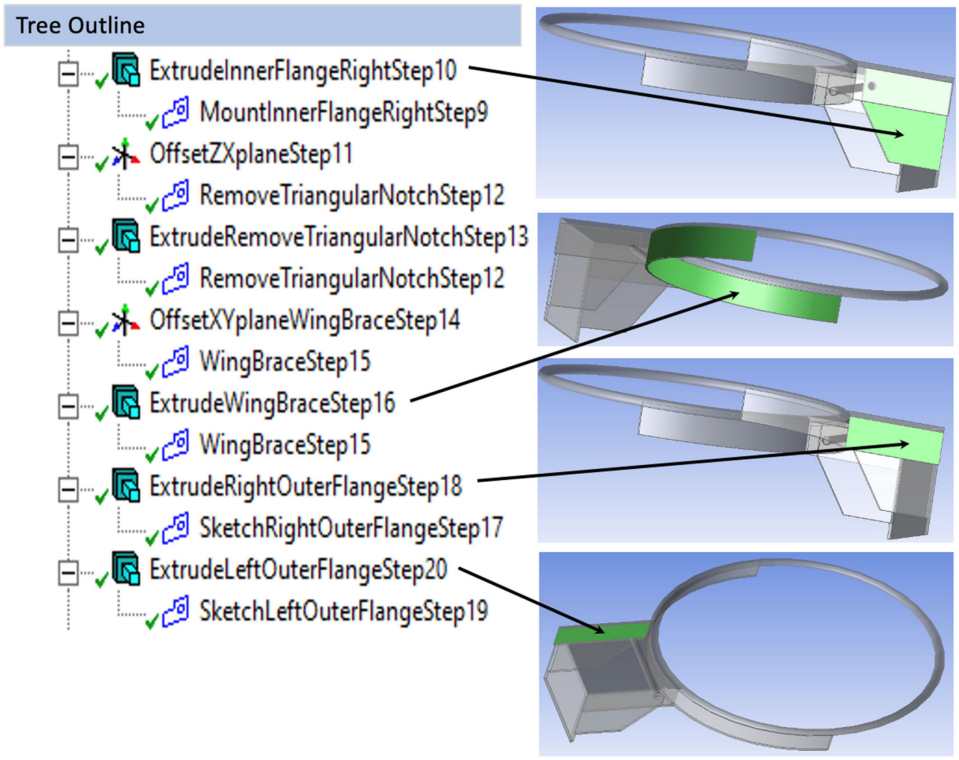


Figure 2. DesignModeler Geometry—Tree Outline 2-of-3.

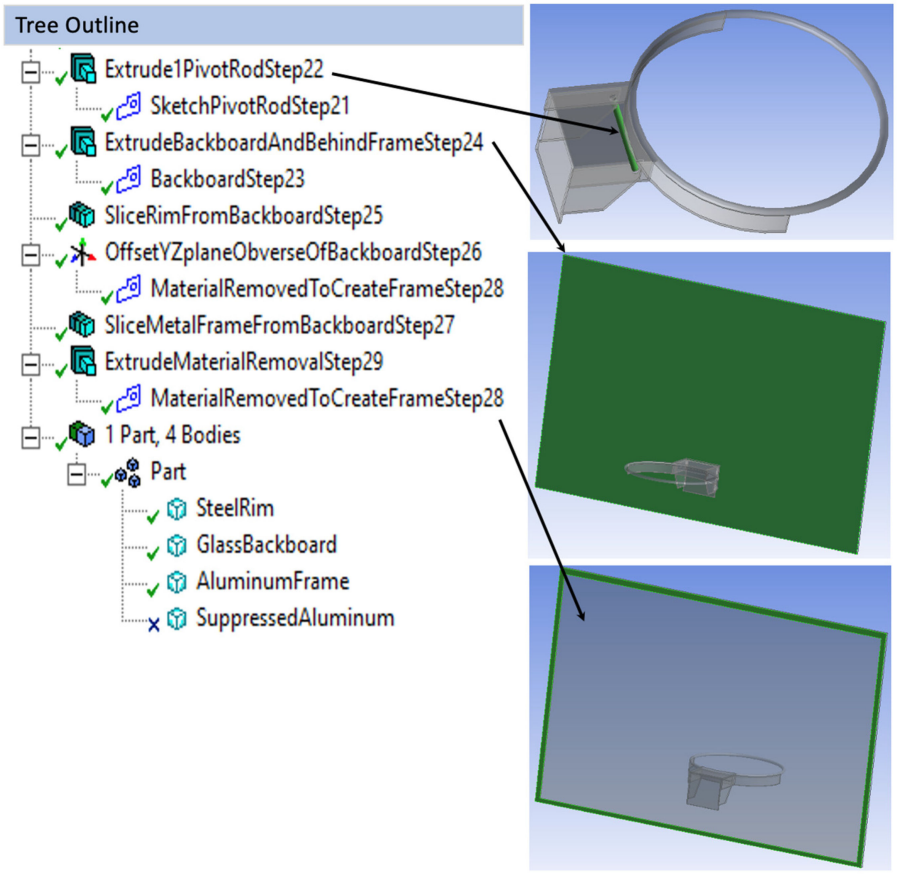


Figure 3. DesignModeler Geometry—Tree Outline 3-of-3.

As shown in Figure 1, the 18-inch internal-diameter toroidal rim was created in step 1 to NCAA specifications [5] and Gared specifications [6]. For this, we used the toroid listed in the create-primitives section. Step 2 was used to create an offset-YZ plane, followed by sketching a rectangle (saw icon) in step 3, then extruding that rectangle from the offset-YZ plane (plane of the backboard) to the toroidal rim to create the top of the mount, step 4, also to NCAA specifications [5] and Gared specifications [6].

Steps 2–4 began a repetitive process shown in Figures 1–3 of sketching a geometry (typically a rectangle) and extruding that geometry, and creating a new plane when needed. For example, the rectangle used to create the back of the mount was defined in step 5, then that rectangle was extruded to create the back of the mount in step 6, to Gared' specifications [6]. Finally, in Figure 1, a rectangle was sketched in step 7 and extruded in step 8 to create the left inner mount flange, also to Gared specifications [6].

In Figure 2, a rectangle was sketched in step 9 and extruded in step 10 to create the right inner mount flange. In step 11, an offset-ZX plane was created, then a sketch of a triangular cutout was made in step 12. In step 13, this triangular cutout was extruded as a material removal, to finalize the five-sided inner flanges. In step 14, a horizontal offset-XY plane was created, then a pair of concentric semicircles were connected at their ends in sketch step 15 before being extruded in step 16 to create the wing brace which attached to the rim. This was followed by sketching a rectangle in step 17 and extruding it in step 18 to form the right outer flange. Then a matching rectangle was created in step 19 and extruded in step 20 to form the left outer flange. Steps 9–20 were performed to match Gared specifications [6]. The wing brace, as well as both the inner and outer flanges, were modeled as 3/16 inch [4.7625 mm] thick steel plate.

In Figure 3, a circle was sketched in step 21 and then extruded in step 22 to form the pivot rod of the break-away release mechanism, matching Gared specifications [6]. This completed the geometric definition of the rim and its mount. Next came a rectangular sketch of the backboard in step 23, and the extrusion of that backboard and its frame in step 24. Step 25 utilized the slice function to separate the rim and its mount from the backboard so that the rim and mount could be declared to be made of steel. Specifically, we used slice—select face—generate. The rim-mound subassembly was then reunited with the backboard by the use of form-new-part to create an assembly of the individual component parts, as shown in Figure 3.

When the backboard was extruded, its thickness was declared to be the thickness of the tempered glass and the thickness of the aluminum frame behind the tempered glass. In step 26, an offset-YZ plane was created so that the metal frame could be sliced from the obverse side of the backboard in step 27. This allowed the backboard to be declared to be made of half-inch [12.7 mm]-thick tempered glass, and the metal frame to be made of aluminum. At this point, the metal frame was a rectangle the same width and height as the backboard. To make the aluminum frame into a border frame, a second slightly smaller rectangle was created in step 28 and extruded as a slice in step 29, to remove unwanted aluminum. This concluded the geometry definition with one part comprising four bodies, the steel rim and mount, the glass backboard, the aluminum border frame, and the material removed from the solid piece of aluminum to make the aluminum border frame. The material removed to create the aluminum border frame was then suppressed to take it out of the analysis; hence the "x" next to it at the bottom left of Figure 3.

Figure 4 gave the major dimensions of the basketball rim and backboard which were used in the steps listed in Figures 1–3. These dimensions, in English inches followed by the respective millimeter equivalents in brackets, came from NCAA specifications [5] and Gared specifications [6], except for the 7.5 inch [190.5 mm] dimension which was measured with calipers. The upper-left top-view in Figure 4 came from Gared [6]. The upper-right top-view and the lower front-view came from our finite element model.

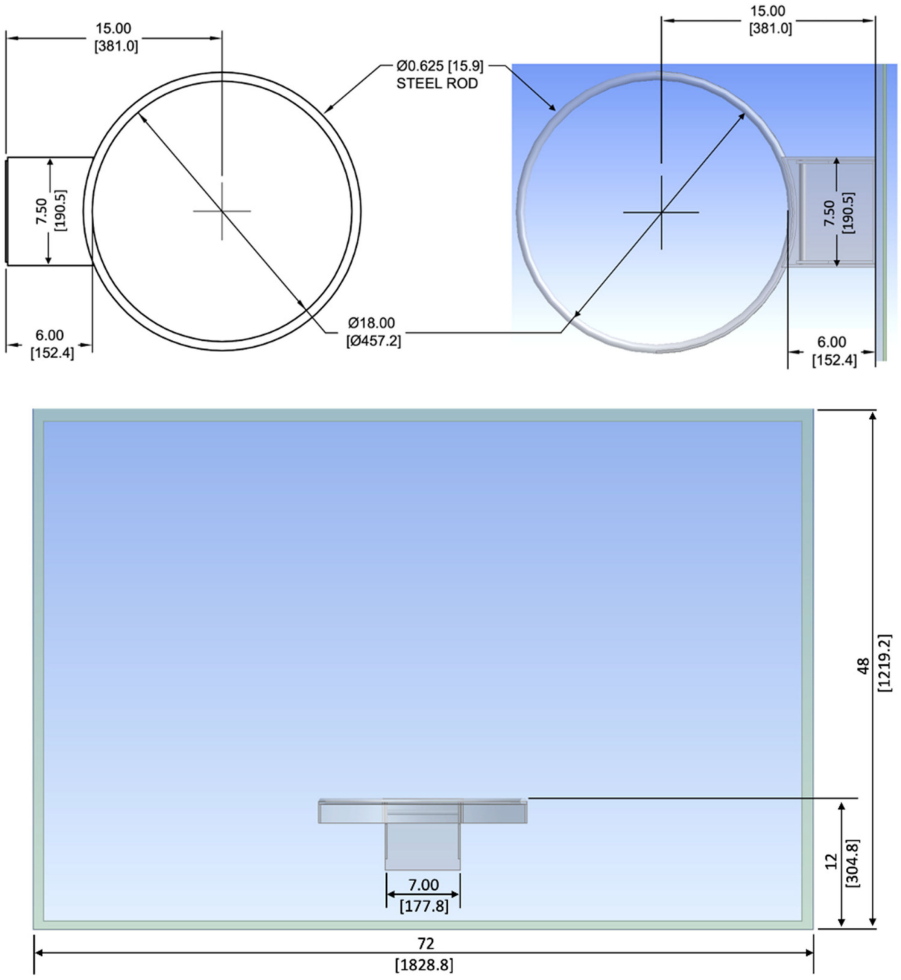


Figure 4. Top and front views of rim and backboard: major dimensions.

The next step was to exit Geometry and enter Model within the MODAL cell. Once in Model, the three-dimensional elements shown in Figure 5 were used to create both meshes seen in Figures 6 and 7. Figure 5 was inspired by the sports-related application of finite elements in [9–13], as these references listed what types of finite elements were used.

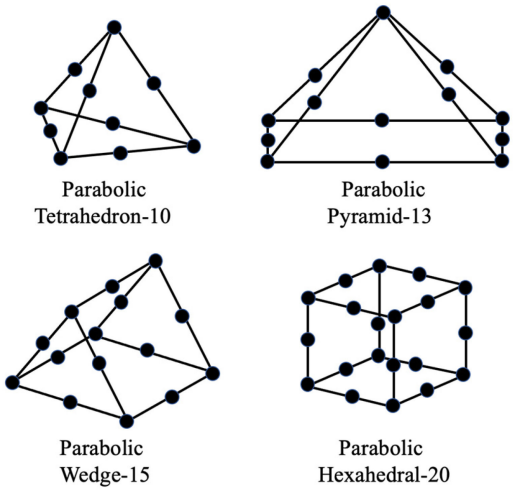


Figure 5. Four parabolic elements.

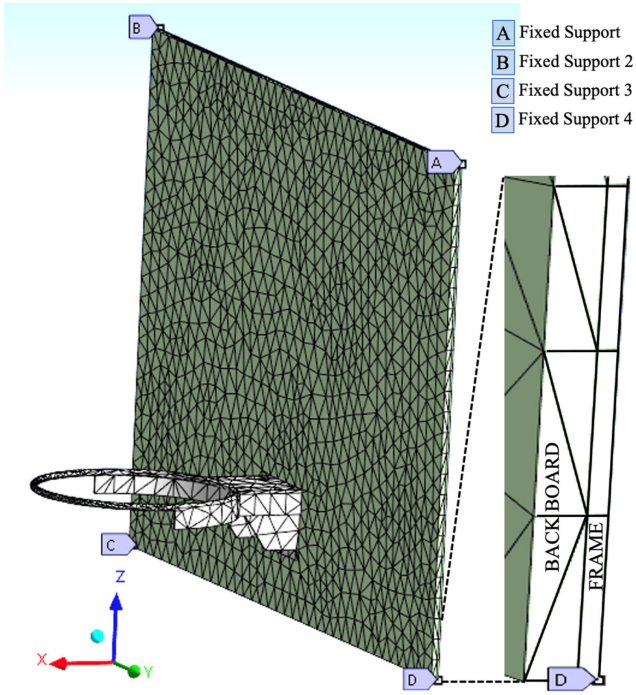


Figure 6. Mesh and fixed supports at corner vertices of aluminum frame.

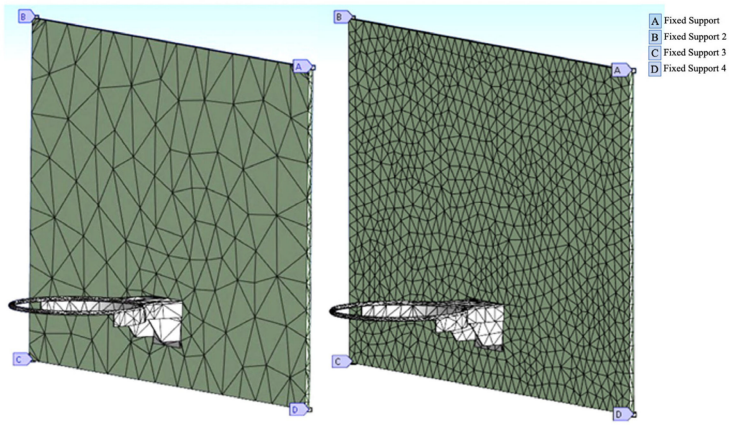


Figure 7. Mesh and fixed supports of 4618-element (**left**) and 8410-element (**right**) models.

The 4618 three-dimensional elements in Table 1, generated by ANSYS mesh parameters set to program default, were all parabolic and comprised a 4218 tetrahedron-10, 196 pyramid-13, 8 wedge-15, and 196 hexahedron-20 elements. As shown in Figure 5, the parabolic tetrahedron element had 4 corner-nodes and 6 mid-nodes, for a total of 10 nodes. The parabolic pyramid element had 5 corner-nodes and 8 mid-nodes, for a total of 13 nodes. The parabolic wedge element had 6 corner-nodes and 9 mid-nodes, for a total of 15 nodes. Finally, the parabolic hexahedral element had 8 corner-nodes and 12 mid-nodes for a total of 20 nodes. Table 1 used a total of 11,200 unique nodes comprising 2218 unique corner-nodes and 8982 unique mid-nodes. The sum of the nodes, corner-nodes, and mid-nodes in the rim and mount, backboard, and frame exceeds the number of unique nodes due to node sharing where these parts interface.

Table 1, above, shows that the rim and mount were originally modeled, using default parameters within ANSYS, with 1979 tetrahedron-10 elements. The backboard was originally modeled with 2239 tetrahedron-10 and 196 pyramid-13 elements, and the aluminum frame was originally modeled with 8 wedge-15 and 196 hexahedral-20 elements.

Table 1. Original-mesh: materials, mesh elements and nodes, and boundary conditions.

Parameter	Rim and Mount (Structural Steel)	Backboard (Tempered Glass)	Frame (6061T6 Aluminum)	Total
Solid (3-D) Elements	1979	2435	204	4618
Nodes	4174	5712	2353	11,200
Corner-Nodes	744	1105	778	2218
Mid-Nodes	3430	4607	1575	8982
Tetrahedron-10	1979	2239		4218
Pyramid-13		196		196
Wedge-15			8	8
Hexahedral-20			196	196
Boundary Conditions			4	4

Table 2, below, shows the changes made via a refined-mesh, where the number of elements was increased by 82%, from 4618 to 8410. Table 2 shows that the rim and mount were then modeled with 2110 (previously 1979) tetrahedron-10 elements. The backboard was then modeled with 6056 (previously 2239) tetrahedron-10 and 120 (previously 196) pyramid-13 elements, and the aluminum frame was then modeled with 4 (previously 8) wedge-15 and 120 (previously 196) hexahedral-20 elements. This mesh refinement was inspired by [9]. Both Tables 1 and 2 were dominated by tetrahedron elements, which was the primary element used in [9].

Table 2. Refined-mesh: materials, mesh elements and nodes, and boundary conditions.

Parameter	Rim and Mount (Structural Steel)	Backboard (Tempered Glass)	Frame (6061T6 Aluminum)	Total
Solid (3-D) Elements	2110	6176	124	8410
Nodes	4412	12,618	1468	17,805
Corner-Nodes	782	2175	488	3173
Mid-Nodes	3630	10,443	980	14,632
Tetrahedron-10	2110	6056		8166
Pyramid-13		120		120
Wedge-15			4	4
Hexahedral-20			120	120
Boundary Conditions			4	4

After the original-mesh and the refined-mesh were separately created, four fixed support conditions were individually applied, one to each of the four outer corner vertices of the aluminum frame behind the backboard, as shown in Figure 6, above. The zoom showing the location of fixed support "D" at an outer corner was equally applicable of fixed supports "A", "B", and "C". The choice of the four fixed support conditions was based on our previously published mode shapes [14] and the support conditions used by Javorski [1]. With the help of the "Details of Mesh" feature of ANSYS, Figure 6 was summarized in Table 1 for the original-mesh and in Table 2 for the refined-mesh. Because elements are not shared between individual parts, the sum of the elements used to model the rim and mount (1979), backboard (2435), and aluminum frame (204) equaled the total (4618) number of elements in Table 1 and the left image in Figure 7. Similarly, the sum of the elements used to model the rim and mount (2110), backboard (6176) and aluminum frame (124) equaled the total (8410) number of elements in Table 2 and the right image in Figure 6.

3. Results

At this point, both the 4618-element and 8410-element finite element models were ready for the calculation of the theoretical mode shapes and frequencies. Figures 8–12 compared our previously published empirically measured frequencies and mode shapes [14] with the theoretical output of the refined-mesh, 8410-element, ANSYS finite element analysis. The bold arrows in Figures 8–12 represented eigenvectors, which were used to explain the relative motions seen in the respective figures.

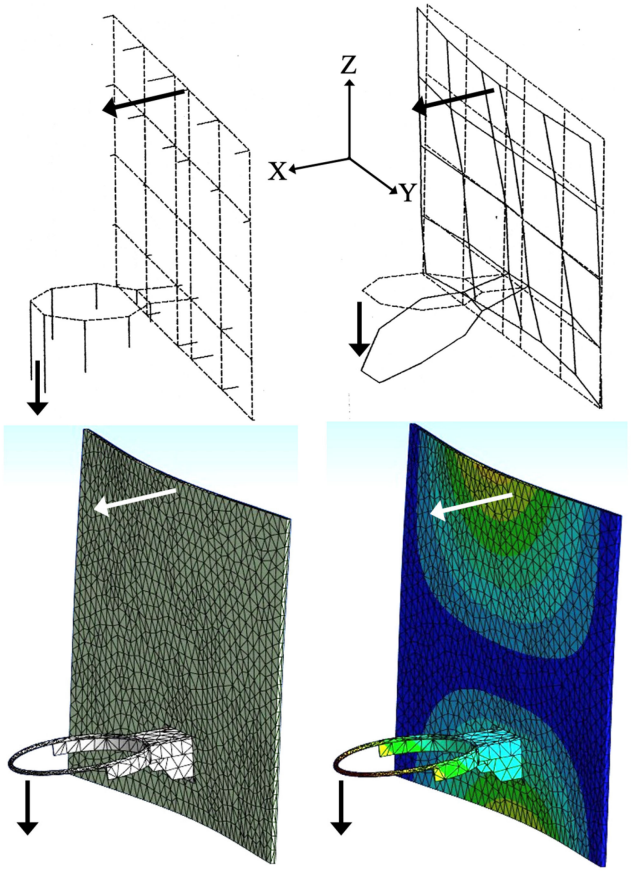


Figure 8. Empirical modal 23.62 Hz (**top**) versus ANSYS FEM 21.328 Hz (**bottom**).

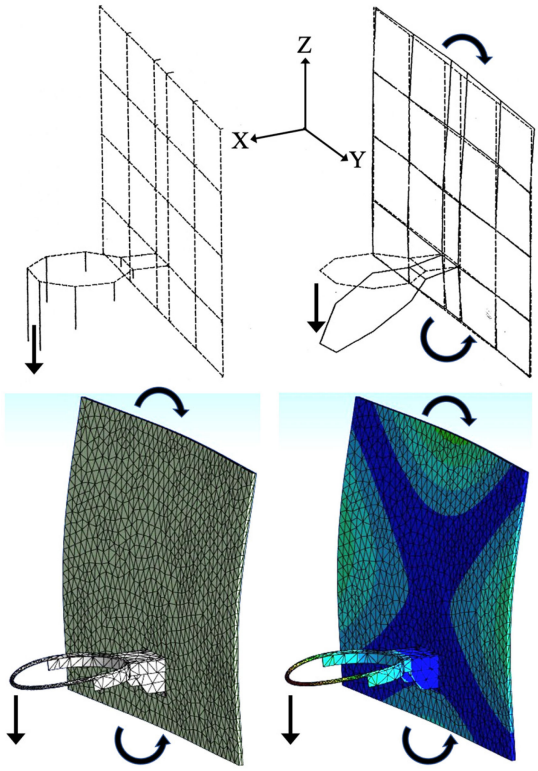


Figure 9. Empirical modal 33.08 Hz (**top**) versus ANSYS FEM 35.888 Hz (**bottom**).

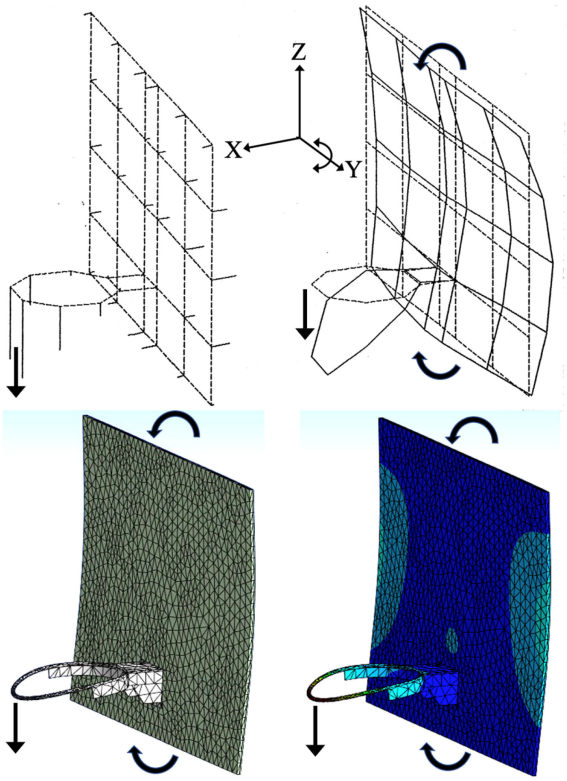


Figure 10. Empirical modal 51.45 Hz (**top**) versus ANSYS FEM 47.177 Hz (**bottom**).

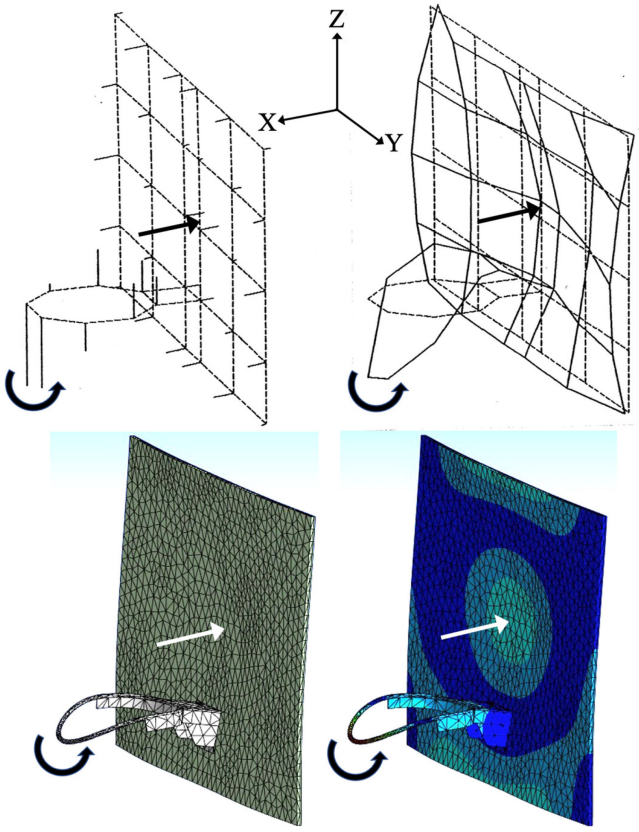


Figure 11. Empirical modal 78.14 Hz (**top**) versus ANSYS FEM 78.028 Hz (**bottom**).

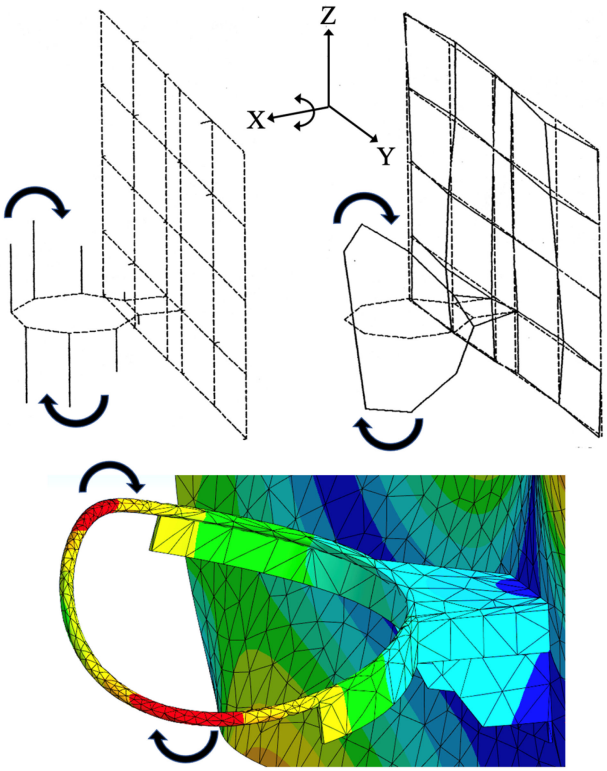


Figure 12. Empirical modal 94.38 Hz (**top**) versus ANSYS FEM 114.81 Hz (**bottom**).

4. Discussion of Results

Figures 8–12 compared our previously published empirically measured frequencies [14] with the theoretical output of the refined-mesh ANSYS finite element analysis, as tabulated in Table 3, below. Table 3 also compared our previously published empirically measured frequencies [14] with the theoretical output of both the original-mesh and the refined-mesh ANSYS finite element analyses.

Table 3. Favorable frequency correlations: original-mesh versus refined-mesh.

	Empirical Modal Analysis [14]	**4618-Element Model (Original-Mesh)**	**8410-Element Model (Refined-Mesh)**
Figure 8	23.62 Hz	22.188 Hz	21.328 Hz
Figure 9	33.08 Hz	37.276 Hz	35.888 Hz
Figure 10	51.45 Hz	50.552 Hz	47.177 Hz
Figure 11	78.14 Hz	83.14 Hz	78.028 Hz
Figure 12	94.38 Hz	131.61 Ha	114.81 Hz
Correlation R		97.187%	98.09%
F		51.076	76.52
SQRT(F)		7.147	8.747
N-2 DOF		3	3
Student-t		7.147 > 5.841	8.747 > 5.841
Confidence		99.5%	99.5%

Figure 8 exhibited an in-phase rocking motion of the rim and backboard, which was indicative of a lower-frequency mode.

Figures 9 and 10 were interesting because the bowing of the backboard in Figure 10 was 180° out of phase from the backboard in Figure 9.

Figure 11 was interesting because both the empirical modal analysis and the theoretical finite element analysis showed that the steel rim was flexing. As the mount and inner portion of the rim flexed upward, the outer portion of the rim flexed downward, and vice

versa. The characteristic oscillating central bulge in the backboard plate prominent in Figure 11 can also be found in [15–18].

Figure 12 was interesting because both the empirical modal analysis and the theoretical finite element analysis showed that the steel rim was twisting in a torsional mode about the X-axis. As stated in [14], the rim was originally modeled as an octagon for the purpose of empirical modal analysis. This offset the fixed-location accelerometer used in the empirical modal analysis from being at the outer end of the rim. Thus, our accelerometer was able to detect the vertical Z motion of this torsion mode.

Using the =PEARSON statistical correlation function in Excel, a correlation between the empirical modal analysis and theoretical ANSYS finite element analysis was calculated at 97.187% for the 4618-element original-mesh, and 98.09% for the 8410-element refined-mesh. A value of 100% would have represented a perfect correlation, a value of 0% would have indicated no correlation, and a value of −100% would have indicated a perfect inverse correlation. The Excel regression function gave a value of F = 51.076 and the square root of F (test statistic) of 7.147 for the original-mesh, and F = 76.52 and the square root of F of 8.747 for the refined-mesh. Using the Student-t distribution for N = 5 sample pairs, with N − 2 = 3 degrees of freedom, showed that 7.147 and 8.747 both exceeded 5.841 [19] which was needed for confidence of 99.5% in both of our correlations. A graphical comparison of the correlation of the theoretical finite element analysis and empirical modal frequencies of the 8410-element refined-mesh model is shown in Figure 13, below.

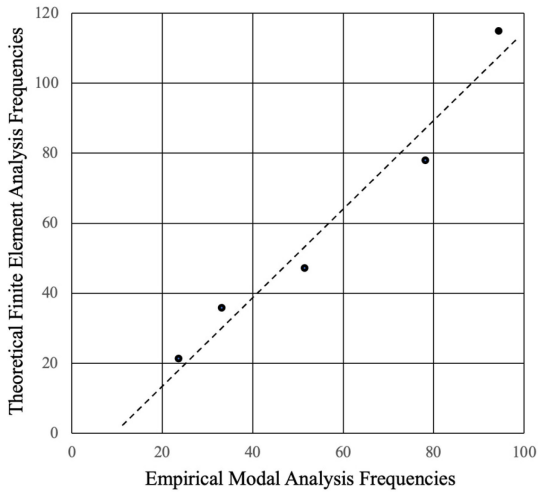


Figure 13. 8410-element model: correlation of theoretical and empirical modal frequencies.

Figures 8–12 all showed that the basketball rim was oscillating perpendicular to the XY (horizontal) plane. As stated in [14], the fixed-location accelerometer used in the empirical modal analysis was near the outer end of the rim and pointed in the vertical Z direction, so the accelerometer would be primarily sensitive to motion perpendicular to the horizontal XY plane. Thus, it is understandable that the theoretical finite element modes shown in Figure 14, below, were missed by the empirical modal analysis because the theoretical motion of the rim in each mode in Figure 14 was entirely within the XY plane.

A video abstract (VA) is available for download to see one complete cycle of vibration for each of Figures 8–12 and 14.

The missed mode at 11 Hz comprised a piston-motion of the rim and mount in the ±X direction. The missed modes at 28 Hz and 44 Hz comprised the reciprocating rotational motion of the rim and mount about the Z-axis. The missed mode at 28 Hz had previously perplexed the authors' empirical modal analysis [14] as that was a common mode of vibrations in plates [16–18]. But we now understand that the lack of vertical motion of the rim in Figure 14 meant that any signal from the vertically oriented accelerometer could have easily been overlooked as noise. This showed us that first obtaining simulation results via finite element analysis could help the planning of subsequent modal analysis experiments.

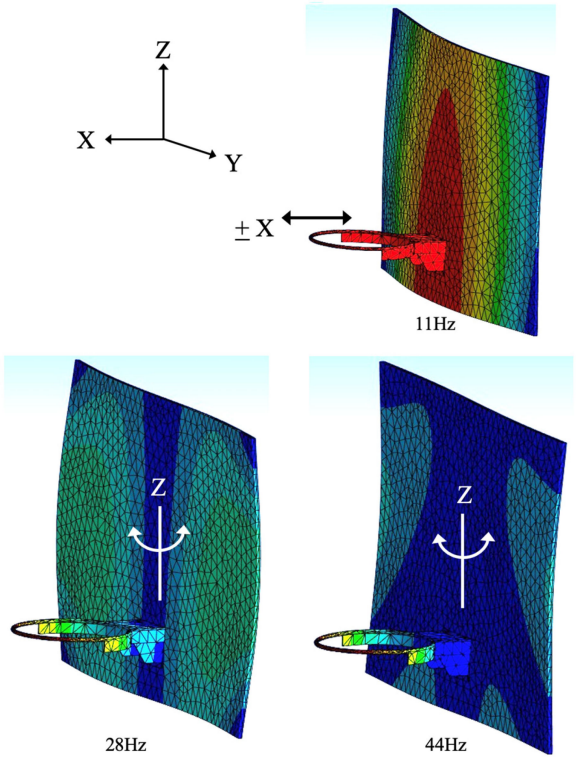


Figure 14. Missed modes predicted by ANSYS FEM at 11, 28, and 44 Hz.

5. Conclusions

Via an ANSYS Tree Outline, 29 steps were documented in detail for the use of the ANSYS MODAL analysis system to create a geometry, mesh, and boundary conditions for a basketball rim, mount, backboard, and border frame.

The purpose of this theoretical finite element analysis was the identification of theoretical modes and frequencies of vibration of one basketball hoop and backboard design. Five empirical modes of vibration compared favorably with this theoretical finite element analysis. These five modes were addressed from a finite element model validation standpoint by statistical correlations with empirical modal analysis data and from a verification standpoint by employing a refined-mesh. The original finite element mesh, generated by default parameters in ANSYS, had a 99.5% confidence in a 97.187% cross-correlation. The refined-mesh, which increased the number of finite elements by 82%, had a 99.5% confidence in a slightly higher 98.09% cross-correlation. The high correlations between the theoretical finite element modeling and the empirical modal analysis were considered a validation of our work. The fact that the refined-mesh did not alter the mode shapes and only made minor changes to the mode frequencies was considered a verification of our finite element model.

There are many possible designs of rims, backboards, and frames which meet NCAA standards, so this study was not comprehensive across the sport of basketball. However, our efforts of finite element analysis did reasonably match empirically measured mode shapes and frequencies of our previously published data. Also, we showed the potential need for a triaxial accelerometer for any future empirical modal analysis efforts involving basketball rims and backboards.

Author Contributions: Conceptualization, K.P.N.; methodology, D.W.; validation, K.P.N., D.W. and T.W.; formal analysis, D.W. and T.W.; investigation, D.W. and T.W.; writing—original draft preparation, D.W.; writing—review and editing, K.P.N., D.W. and T.W.; visualization, K.P.N. and D.W.; supervision, K.P.N.; project administration, K.P.N. All authors have read and agreed to the published version of the manuscript.

Funding: This research received no external funding.

Data Availability Statement: The archived 2024R1 Work Bench Project Zip file, *.wbpz, with all ANSYS commands used in this paper, will be freely available through MDPI.

Acknowledgments: Donna Robinson Winarski is acknowledged for her support of this research, both at the United States Military Academy at West Point, New York, and at Tucson, Arizona. Her assistance with initial editing as well as data taking was very much appreciated.

Conflicts of Interest: The authors declare no conflicts of interest.

References

1. Javorski, M.; Čermelj, P.; Boltežar, M. Characterization of the Dynamic Behaviour of a Basketball Goal Mounted on a Ceiling. *J. Mech. Eng./Stroj. Vestn.* **2010**, *56*, 497.
2. Finite Element Analysis, Cornell Certificate Program. Available online: https://ecornell.cornell.edu/certificates/engineering/finite-element-analysis/ (accessed on 24 January 2024).
3. ANSYS 2024 R1 Student Edition. Available online: https://www.ansys.com/academic/students/ansys-student (accessed on 30 January 2024).
4. Tickoo, S. *ANSYS Workbench 2023 R2: A Tutorial Approach*; CADCIM Technologies: Schererville, IN, USA, 2023; pp. 5-24–5-37.
5. 2023–2024 NCAA Men's Basketball Rules Handbook, Updated 27 November 2023. Manuscript Prepared By: Jeff O'Malley, Secretary-Rules Editor, NCAA Men's Basketball Rules Committee. Edited By: Andy Supergan, Assistant Director of Playing Rules and Officiating. Available online: https://www.ncaapublications.com/productdownloads/BK24-20231127.pdf (accessed on 22 February 2024).
6. Model 3500 Positive Lock Breakaway Goal. Updated 21 January 2010. Gared Holdings, LLC. Available online: https://www.garedsports.com/sites/default/files/import/files/3500I%2520spec%2520-revA.pdf (accessed on 7 September 2023).
7. Nkounhawa, P.K.; Ndapeu, D.; Kenmeugne, B.; Beda, T. Analysis of the Behavior of a Square Plate in Free Vibration by FEM in Ansys. *World J. Mech.* **2020**, *10*, 11–25. [CrossRef]
8. Guguloth, G.N.; Singh, B.N.; Ranjan, V. Free vibration analysis of simply supported rectangular plates. *Vibroeng. Procedia* **2019**, *29*, 270–273. [CrossRef]
9. Covill, D.; Drouet, J.-M. On the Effects of Tube Butting on the Structural Performance of Steel Bicycle Frames. *Proceedings* **2018**, *2*, 216.
10. Tanaka, K.; Sekizawa, K. Construction of a finite element model of golf clubs and influence of shaft stiffness on its dynamic behavior. *Proceedings* **2018**, *2*, 247.
11. Matsuda, A.; Nakui, M.; Hashiguchi, T. Simulation of Mechanical Characteristics of Tennis Racket String Bed Considering String Pattern. *Proceedings* **2018**, *2*, 264.
12. Takizawa, M.; Matsuda, A.; Hashiguchi, T. A Study on the Mechanical Characteristics of String Planes of Badminton Racquets by Nonlinear Finite Element Analysis. *Proceedings* **2020**, *49*, 42.
13. Yin, S.-R.; Chang, H.-C.; Cheng, K.B. Impact Characteristics of a Badminton Racket with Realistic Finite Element Modeling. *Proceedings* **2020**, *49*, 106.
14. Winarski, D.; Nygren, K.P.; Winarski, T. Modes of Vibration in Basketball Rims and Backboards and the Energy Rebound Testing Device. *Vibration* **2023**, *6*, 726–742. [CrossRef]
15. Irvine, T. The Natural Frequency of a Rectangular Plate Point-Supported at Each Corner, Revision C. 1 August 2011. Available online: http://www.vibrationdata.com/tutorials2/plate_point_corner.pdf (accessed on 25 July 2023).
16. Dumond, P.; Monette, D.; Alladkani, F.; Akl, J.; Chikhaoui, I. Simplified setup for the vibration study of plates with simply-supported boundary conditions. *Methods X* **2019**, *6*, 2106–2117. [CrossRef] [PubMed]
17. Anđelić, N.; Čanađija, M.; Car, Z. Determination of Natural Vibrations of Simply Supported Single Layer Graphene Sheet using Non-Local Kirchhoff Plate Theory. In Proceedings of the IN-TECH 2017 International Conference on Innovative Technologies, Ljubljana, Slovenia, 11–13 September 2017; p. 5.
18. Geveci, B.; Walker, J.D.A. Nonlinear resonance of rectangular plates. *Proc. R. Soc. Lond. Ser. A Math. Phys. Eng. Sci.* **2001**, *457*, 1215–1240. [CrossRef]
19. Devore, J.L. *Probability and Statistics for Engineering and the Sciences*, 4th ed.; Brooks/Cole Publishing: Pacific Grove, CA, USA, 1995; p. 707.

Disclaimer/Publisher's Note: The statements, opinions and data contained in all publications are solely those of the individual author(s) and contributor(s) and not of MDPI and/or the editor(s). MDPI and/or the editor(s) disclaim responsibility for any injury to people or property resulting from any ideas, methods, instructions or products referred to in the content.